Effect of mobility on collective phase dynamics of nonlocally coupled oscillators with a phase lag

Bojun Li and Nariya Uchida*
Department of Physics, Tohoku University, Sendai 980-8578, Japan

(Received 28 August 2022; accepted 2 November 2022; published 15 November 2022)

Nonlocally coupled oscillators with a phase lag self-organize into various patterns, such as global synchronization, the twisted state, and the chimera state. In this paper, we consider nonlocally coupled oscillators that move on a ring by randomly exchanging their positions with the neighbors and investigate the combined effects of phase lag and mobility on the collective phase dynamics. Spanning the whole range of phase lag and mobility, we show that mobility promotes synchronization for an attractive coupling, whereas it destroys coherence for a repulsive coupling. The transition behaviors are discussed in terms of the timescales of synchronization and diffusion of the oscillators. We also find a novel spatiotemporal pattern at the border between coherent and incoherent states.

DOI: 10.1103/PhysRevE.106.054210

I. INTRODUCTION

Collective synchronization is observed in a wide range of natural phenomena, such as flashing fireflies, cardiac beats, and circadian rhythms [1]. Although a global coupling explains the emergence of fully synchronized states [2], a nonlocal (or finite-range) coupling introduces the twisted and the chimera states. The twisted state [3,4] is a state in which the phase difference between two successive oscillators in a linear array is constant. The chimera state [5] is characterized by spatial coexistence of coherent and incoherent groups of oscillators, which was discovered by introducing a phase lag in the nonlocal coupling [6]. It has been a target of extensive studies in the past decade [7,8], realized in various physical systems, and its relevance to neuronal activities is recently attracting attention [9,10]. These states are most simply described by the phase oscillators on a linear array, the time evolution of which obeys

$$\dot{\phi}(x,t) = \omega_0 - \sum_{x' \neq x} g(x-x') \sin[\phi(x,t) - \phi(x',t) + \alpha\pi], \tag{1}$$

where $\phi(x,t)$ is the phase at position x and time t, ω_0 is the intrinsic phase velocity, $g(x)$ is the interaction kernel, and $\alpha\pi$ is the phase lag (we assume $0 \leqslant \alpha \leqslant 1$ without loss of generality). The phase lag induces frustration in the system which gives rise to a variety of intriguing patterns. For $\alpha < 0.5$, the coupling is attractive. If α is sufficiently small, the system that started from a random initial condition eventually reaches a coherent state (either a synchronous or a twisted state). When α exceeds a threshold, the frustration destroys coherence and forms a chimera state or a multichimera state with many coherent and incoherent regions [11]. The onset of the multichimera state is a critical transition that resembles directed percolation [12,13]. For a repulsive coupling ($\alpha > 0.5$), we find coexistence of twisted states with positive and negative phase differences separated by incoherent strips [14]. A randomly branching multichimera state disappears at an upper threshold of α and is replaced by stripe patterns with smooth boundaries. For α close to unity, frequency synchronization takes place in the coexisting twisted states.

Another interesting situation is brought by the oscillators that move in space and change the partners to interact with. Mobile oscillators are related to biological phenomena including animal groups [15] and chemotactic elements [16] and have potential technological applications, i.e., in robotics [17,18] and wireless sensor networks [19]. The effect of mobility on synchronization has been an actively studied subject in the past decade [20–31]. In Ref. [20], it was shown that mobility destabilizes the twisted states and promotes synchronization. Reference [22] shows that mobility speeds up synchronization by extending the effective coupling range. Reference [27] studied the system with a delayed coupling and found that mobility can induce chimera states. Reference [28] considered mobile oscillators with mutual interaction between motion and phase and found a variety of nontrivial swarming and synchronized patterns. However, little is known about the combined effects of phase lag and mobility on the twisted and chimera states. Two recent studies considered the system with a phase lag: Ref. [29] demonstrated the transition between the synchronous state and the chimera states with one or two coherent regions; Ref. [31] shows that disorder of the oscillators facilitates stability of chimera. These papers focus on a system with the phase lag α close to 0.5, and a study spanning a wide range of α is still lacking.

In this paper, we investigate the combined effects of phase lag and mobility on the collective phase dynamics of nonlocally coupled oscillators on a ring. We span the whole range of phase lag and mobility and find that mobility promotes synchronization for an attractive coupling, whereas it destroys coherence for a repulsive coupling. The transition behaviors are discussed in terms of the timescales of synchronization and diffusion of the oscillators. For the attractive case, we

*uchida@cmpt.phys.tohoku.ac.jp

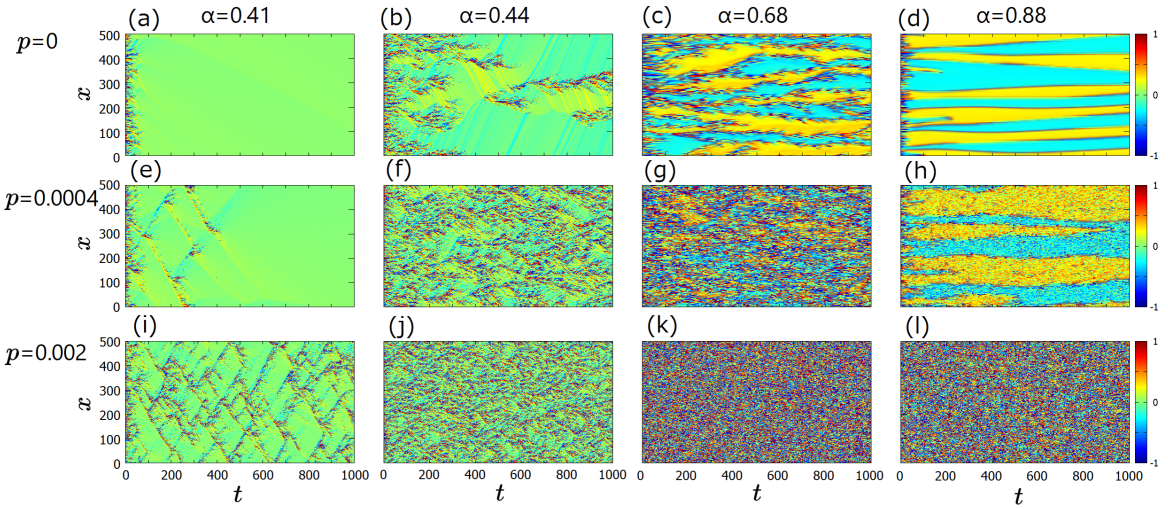

FIG. 1. Spatiotemporal patterns of the phase difference $\Delta(x,t)$, for $\alpha = 0.41, 0.44, 0.68, 0.88$ from the left to the right column, and $p = 0, 0.0004, 0.002$ from the top to the bottom row.

estimate the size of the basins of attraction for the synchronous and twisted states and characterize the collapse of the twisted states into the synchronous states quantitatively. We also find a novel meshlike pattern that consists of intersecting traveling waves near the coherent-chimera transition. For the repulsive case, mobility induces noisy patches of twisted states, which gradually crosses over to a fully incoherent state as the mobility is increased.

II. MODEL

We consider N oscillators that are distributed on a ring with N sites labeled by the integer coordinates x (mod N). Each site on the ring is occupied by a single oscillator at a time. The model is built upon Eq. (1) for non-mobile oscillators with the interaction kernel,

$$g(x)\begin{cases} = \dfrac{1}{2R} & (|x| \leqslant R), \\ = 0 & (|x| > R), \end{cases} \tag{2}$$

where R is the coupling range. The intrinsic frequency ω_0 is set to zero without losing generality. The oscillators move stochastically by exchanging their positions with their nearest neighbors at a constant rate. It is implemented by a discrete dynamical rule with a small time step δt. At each time step, each oscillator exchanges its position with its right nearest neighbor with the probability p, which causes the change in phases $\phi(x, t+\delta t) = \phi(x+1, t)$ and $\phi(x+1, t+\delta t) = \phi(x, t)$. Since the average number of moves of each oscillator during one time unit is $2p/\delta t$, the mean square displacement is given by

$$\langle(\Delta x)^2\rangle \equiv \langle[x(t'+t) - x(t')]^2\rangle = \frac{2p}{\delta t}t, \tag{3}$$

and the diffusion constant is $D = p/\delta t$. Thus, the model is characterized by three parameters R, α, and p.

We solve Eq. (1) using the Runge-Kutta method with a time step 0.01. Unless otherwise stated, we set $R = 5$ and $N = 500$. Uniformly random values of the phases are used for the initial condition. The mobility is implemented by randomly choosing a site x and exchanging the phases of the oscillators at x and $x+1$ with the probability p. This process is repeated N times at each time interval δt, which is also set to 0.01. We checked that a smaller value of δt does not significantly change the results presented in the next section.

III. NUMERICAL RESULTS

A. Spatiotemporal patterns and the strength of incoherence

In Fig. 1, we plot the spatiotemporal patterns of the phase difference between two neighbor oscillators $\Delta(x,t) = [\phi(x+1,t) - \phi(x,t)]/\pi$, truncated in the range $[-1{:}1)$. The first row shows the patterns for $p = 0$ with α varied. We varied α in the range of $0 \leqslant \alpha < 1$, and only a few samples are shown. For $\alpha < 0.44$, the system reaches a coherent state with a uniform and very small value of Δ [Fig. 1(a)]. For $0.44 \leqslant \alpha < 0.5$, incoherent regions unceasingly branch and disappear, forming a multichimera state [12,13] [Fig. 1(b)]. For a repulsive coupling ($\alpha > 0.5$), twisted states with positive and negative values of Δ are separated by incoherent strips of width $\propto R$; for α not far from 0.5, a randomly branching multichimera state appears [Fig. 1(c)] which is replaced by coexisting twisted states with smooth boundaries for a larger α [Fig. 1(d)] [14].

The mobility of the oscillators introduces a novel spatiotemporal pattern. The patterns for $p = 0.0004$ and 0.002 are shown in the second and third rows of Fig. 1, respectively. For $0.38 \leqslant \alpha < 0.44$, we find a meshlike pattern that consists of intersecting traveling waves [Figs. 1(e)–1(i)]. The chimera state for $\alpha = 0.44$ obtains finer structures of incoherent regions due to the mobility [Figs. 1(f)–1(j)]. For $\alpha > 0.5$, noisy spots are added to the multichimera states [Figs. 1(g) and 1(h)]. At $p = 0.002$, the patterns are further randomized, and we cannot recognize the original patterns for $p = 0$ [Figs. 1(k) and 1(l)].

As a measure of the strength of incoherence, we follow a previous work [32] and use the standard deviation of the phase

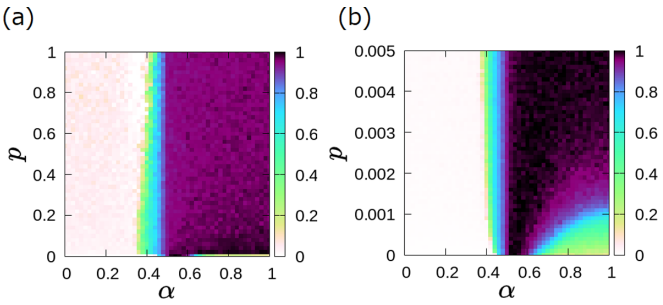

FIG. 2. The strength of incoherence $\overline{\sigma_\Delta}$ on the (α, p) plane, for (a) $0 \leqslant p < 1$ and (b) $0 \leqslant p < 0.005$. The color scale (grayscale) shows a coherent state ($\overline{\sigma_\Delta} \ll 1$) in light (whitish) colors, and an incoherent state ($\overline{\sigma_\Delta} \sim 1$) in dark colors (black and dark gray).

difference within a distance R from the site x,

$$\sigma_\Delta(x,t) = \sqrt{\frac{3}{2R}\sum_{x'=x-R}^{x+R-1}[\Delta(x,t) - \overline{\Delta}(x,t)]^2}, \tag{4}$$

where $\overline{\Delta}(x,t)$ is the phase difference averaged over the interval $[x-R, x+R]$ and the prefactor is chosen to make the maximum value of $\sigma_\Delta(x,t)$ equal to 1. The strength of incoherence of the whole system is written as $\overline{\sigma_\Delta}(t) = \langle \sigma_\Delta(x,t)\rangle_x$. Figure 2 shows the value of $\overline{\sigma_\Delta}(t)$ at $t = 1000$ averaged over ten independent samples for each set of (α, p). The entire range of the mobility ($0 \leqslant p \leqslant 1$) is shown in Fig. 2(a) and a magnified view of the range $0 \leqslant p \leqslant 0.005$ is shown in Fig. 2(b). We obtain coherent states ($\overline{\sigma_\Delta} \ll 1$) for small α irrespective of the value of p. The degree of incoherence sharply increases at $\alpha = \alpha_c \simeq 0.4$, and the threshold α_c has a minor dependence on p. On the other hand, when $\alpha > 0.5$, the system falls into complete incoherence ($\overline{\sigma_\Delta} \sim 1$) over most of the parameter range except for very small p. These changes brought by the mobility will be further discussed in the following sections.

B. The effect of mobility on the coherent states

We first focus on the effect of mobility on the coherent states for $\alpha < \alpha_c(p)$. In this parameter range, the system is multistable, i.e., either the synchronous or q-twisted states are achieved depending on the initial condition. The phase difference in these states can be written as $\Delta = 2q/N$, where $q = 0$ represents the synchronous state, and a nonzero integer with $|q| \leqslant \frac{N-1}{2}$ corresponds to the q-twisted state.

In the simulation, we compute the winding number q as

$$q = \frac{1}{2}\sum_{x=1}^{N}\Delta(x,t), \tag{5}$$

with $t = 1000$. We take an average over 100 samples for each value of (α, p) unless otherwise stated, including the incoherent states where $\Delta(x,t)$ is not spatially uniform. We also measure the root mean square (rms) of q, which is denoted by σ_q. Figure 3 shows the histograms of q for specific values of (α, p). For $p = 0$, the distribution is wide, and the maximum value of $|q|$ reaches 6. As p increases, the distribution becomes narrower, which means that the mobility enlarges the size of

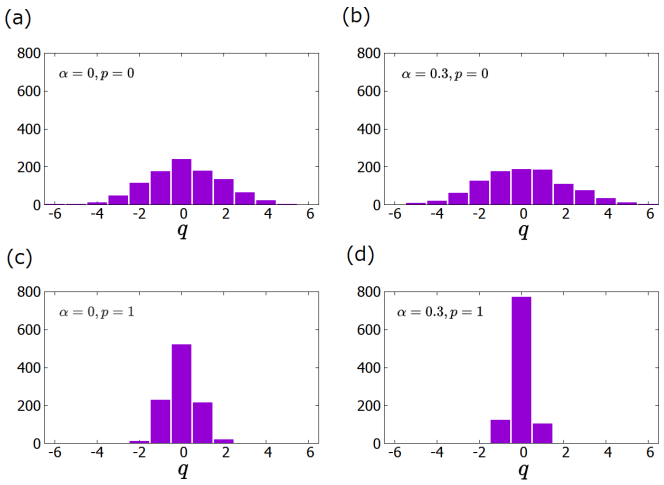

FIG. 3. Histograms of the winding number q for 1000 independent samples. (a) $(\alpha, p) = (0, 0)$, which gives $\sigma_q = 1.79$, (b) $(\alpha, p) = (0.3, 0)$, $\sigma_q = 2.02$. (c) $(\alpha, p) = (0, 1)$, $\sigma_q = 0.76$. (d) $(\alpha, p) = (0.3, 1)$, $\sigma_q = 0.48$.

the basin of attraction for a smaller value of $|q|$. For $p = 1$, the peak for $\alpha = 0.3$ is higher than the one for $\alpha = 0$. It means that the phase lag widens the basin of attraction of the synchronous state. Note that the estimated size of the basin of attraction might contain errors due to finite simulation time and finite number of initial conditions sampled, although we checked that temporal evolution of q almost ceased at $t = 100$ for typical cases. A more sophisticated sampling method [33] would be useful for an accurate estimate of the asymptotic behavior for large $|q|$.

Figure 4(a) shows the rms of the winding number on the (α, p) plane. We focus on the coherent (synchronous or q-twisted) states with $\alpha < \alpha_c(p)$ here. The rms decreases as α and p increase in the coherent region of the (α, p) plane. Notably, it becomes almost zero at large p and near $\alpha = \alpha_c(p)$ [Fig. 4(c)], which means that the synchronous state $q = 0$

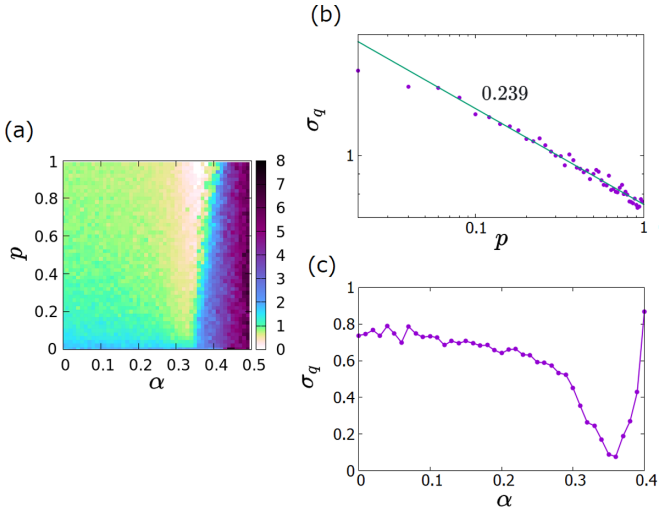

FIG. 4. (a) The rms of the winding number σ_q for each (α, p). (b) The rms σ_q versus p for $\alpha = 0$. (c) The rms σ_q versus α for $p = 1$. The data in (b) and (c) are averages over 1000 independent samples.

is attained for most of the samples. In Fig. 4(b), we plot σ_q for $\alpha = 0$ as a function of the mobility parameter p. It is fitted by the power law $\sigma_q \sim p^{-\beta}$ with the exponent $\beta = 0.239 \pm 0.005$ in the range of $0.1 \leqslant p \leqslant 1$. We will discuss in Sec. IV the reason why the exponent is close to 1/4.

The enhancement of synchronization by the mobility is explained by disturbance of the q-twisted states. The exchange of two oscillators in a twisted state alters the phase differences at three successive sites from $\{\Delta, \Delta, \Delta\}$ to $\{2\Delta, -\Delta, 2\Delta\}$. The total change in the phase differences is 4Δ, and is larger for a larger $|q|$ because $\Delta = 2q/N$. Conversely, a twisted state with a smaller $|q|$ is less affected, and the fully synchronized state is unchanged by the exchange. If the disturbance due to mobility dominates the effect of interaction to recover the initial (twisted) state, the system leaves the basin of attraction and hops to another as already shown for $\alpha = 0$ [3]. In the following, we analyze the balance between the effects of mobility and coupling quantitatively by computing the timescales to disturb and restore the twisted states.

A system in a q-twisted state is divided into $|q|$ blocks of size $N/|q|$. In each block, the phase changes by 2π. In the absence of coupling, the time required for the phase differences to be randomized should be proportional to the time for each oscillator to travel the distance of $N/|q|$, the size of a block. Substituting $N/|q|$ into Δx in the left side of Eq. (3), the characteristic time for the randomization is written as

$$\tau_{\rm rand} \sim \frac{N^2 \delta t}{2pq^2}. \tag{6}$$

In order to quantitatively estimate the timescale, we consider a system that has only the mobility but no phase coupling. We analyze the spatial correlation of the phase difference using the function,

$$G_\Delta(x,t) = \langle \cos\, \pi[\Delta(x'+x,t) - \Delta(x',t)]\rangle_{x'}. \tag{7}$$

Here the average is taken over x' and 100 independent samples. Note that the function has the maximal value of 1 when the phase difference is spatially uniform and that it vanishes if the phase difference is spatially random. We choose the q-twisted state as the initial condition. In this case, the function has little dependence on x because the phase difference is uniform in the initial state, and the randomization takes place uniformly. Therefore, we use the data for $x = N/2$ in the following, and write it as $G_\Delta(t)$. As shown in Figs. 5(a) and 5(b), $G_\Delta(t)$ decays exponentially in a wide range of p and q. By fitting $G_\Delta(t)$ by an exponential function, we get

$$G_\Delta(t) = \exp\left(-\frac{2pq^2}{a^2N^2\delta t}t\right), \tag{8}$$

with the coefficient $a \approx 0.11$. Now we redefine the timescale for randomization $\tau_{\rm rand}$ by $G_\Delta(\tau_{\rm rand}) = 0.1$, which gives

$$\tau_{\rm rand} \approx 1.4 \times 10^{-4}\frac{N^2}{pq^2}. \tag{9}$$

On the other hand, the coupling between oscillators tends to restore the twisted states. We turned off the mobility and calculated the strength of incoherence $\overline{\sigma_\Delta}$ as a function of time, starting from random states; see Fig. 5(c) for an attractive coupling ($0 \leqslant \alpha \leqslant 0.4$) and (d) for a repulsive coupling

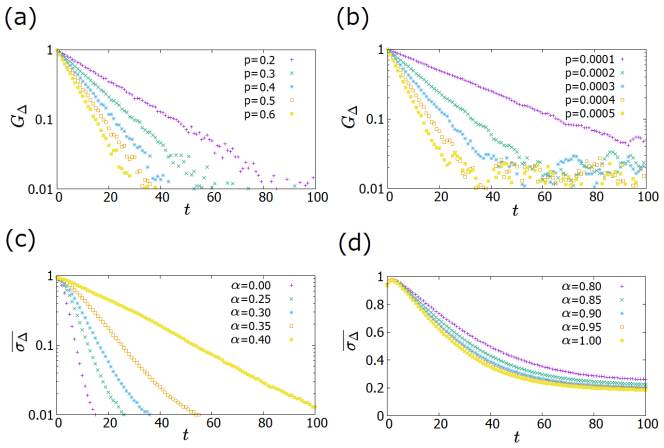

FIG. 5. (a) and (b) Temporal decay of coherence is measured by the function $G_\Delta(N/2,t)$ for a system without the coupling. It is obtained by starting from the q-twisted state with (a) $q = 2$ and (b) $q = 67$. It shows the effect of mobility to randomize the phase difference. (c) and (d) The strength of incoherence $\overline{\sigma_\Delta}$ obtained without mobility and starting from the random state for (c) $0 \leqslant \alpha \leqslant 0.4$ and (d) $0.8 \leqslant \alpha \leqslant 1$. It shows the effect of coupling to restore the q-twisted states.

($0.8 \leqslant \alpha \leqslant 1$). In the attractive case, the decay of $\overline{\sigma}_\Delta$ is slower for larger α, which is interpreted as the result of the frustration introduced by the phase lag. We define the timescale for restoring coherence $\tau_{\rm coh}$ as the time for $\overline{\sigma_\Delta}$ to decrease from 1 to 0.1. Figure 6(a) shows that $\tau_{\rm coh}$ increases as α is increased from 0 to 0.4.

Now we compare the timescales $\tau_{\rm rand}$ and $\tau_{\rm coh}$ to analyze the competition between the mobility and coupling. In Fig. 6(b), we plot $\tau_{\rm rand}$ given by Eq. (9) for $q = 1, 2$ with solid lines and $\tau_{\rm coh}$ for $\alpha = 0, 0.3, 0.4$ with dashed lines. For $\alpha = 0$, we have $\tau_{\rm coh} = 7.4$, and it is smaller than $\tau_{\rm rand}$ for all p and for $q = 1, 2$. This is in agreement with the result that the q-twisted states with $q = 1$ and 2 are stable up to $p = 1$ [Fig. 3(c)]. For $\alpha = 0.3$, we get $\tau_{\rm coh} = 16.6$, which exceeds $\tau_{\rm rand}$ for $q = 2$ when $p \gtrapprox 0.5$. This suggests that the twisted state with $q = 2$ is unstable, whereas the twisted state with $q = 1$ is still stable for all p's, which is also consistent with the full numerical results [Fig. 3(c)]. For $\alpha = 0.4$ and large p, $\tau_{\rm coh} = 54.0$ is smaller than $\tau_{\rm rand}$ even for $q = 1$, which explains the result that only the synchronized state remains

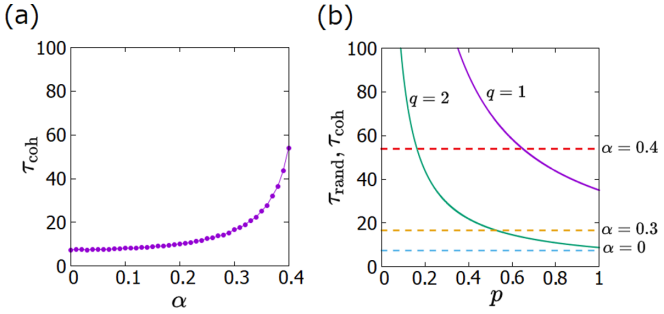

FIG. 6. (a) The timescale for restoring coherence $\tau_{\rm coh}$ versus α. (b) Comparison of the timescales. Solid lines: $\tau_{\rm rand}$ for $q = 1, 2$. Dashed lines: $\tau_{\rm coh}$ for $\alpha = 0, 0.3, 0.4$.

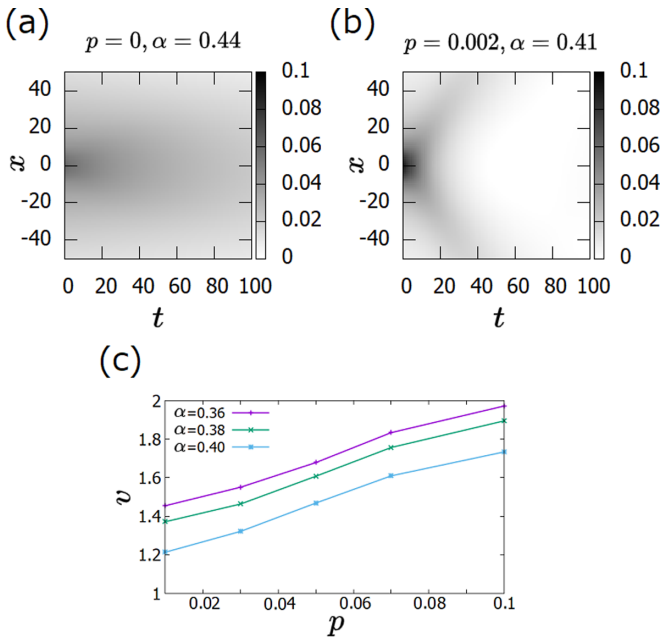

FIG. 7. The spatiotemporal correlation function $G_\sigma(x,t)$ for (a) $(\alpha, p) = (0.44, 0)$, and (b) $(\alpha, p) = (0.41, 0.002)$, which corresponds to the patterns in Figs. 1(b) and 1(i), respectively. The gray scale represents the strength of correlation. (c) The average speed of the traveling wave v_w versus p.

stable [Fig. 4(a)]. Thus we have shown that the stability of the q-twisted states for $\alpha < \alpha_c(p)$ is determined by the competition between mobility and coupling, and that the two timescales that are measured separately can explain the result: the q-twisted state is unstable if the disturbance caused by the mobility is faster and is stable if the recovery of coherence by the coupling is faster.

C. Traveling waves in the transition region

We next consider the effect of mobility in the transition region just above $\alpha = \alpha_c(p)$, where the strength of incoherence $\overline{\sigma_\Delta}$ is between 0 and 1. The spatiotemporal patterns obtained in this range is characterized by the spatiotemporal correlation function of σ_Δ,

$$G_\sigma(x,t) = \langle \sigma_\Delta(x',t')\sigma_\Delta(x'+x,t'+t) - \sigma_\Delta^2(x',t')\rangle_{x',t'}. \tag{10}$$

In Fig. 7, we show this function computed in the time window $500 < t' < 1000$ and averaged over 100 independent samples.

For $p = 0$, the randomly branching pattern of incoherent states [Fig. 1(b)] gives the monotonically decaying correlation function in Fig. 7(a). For $p > 0$, the meshlike pattern consisting of intersecting traveling waves [Fig. 1(i)] gives the V-shaped correlation pattern in Fig. 7(b). In order to measure the speed of the traveling waves, we identify the average trajectory $x_w(t)$ of each traveling wave with the "ridge" of the correlation function, where $G_\sigma(x,t)$ is maximal for each t. The average speed v_w of the traveling wave is measured by fitting $x_w(t)$ with a line. The dependence of v_w on the mobility p is shown in Fig. 7(c). The speed linearly increases with p, and slightly decreases as α is increased above α_c.

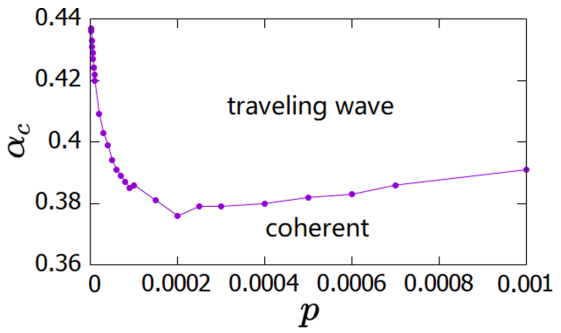

FIG. 8. The transition threshold $\alpha_c(p)$. For $\alpha < \alpha_c$, only the coherent states remain in the long-time limit, whereas traveling waves appear for $\alpha > \alpha_c$.

We define the threshold α_c as the smallest value of α for which $\overline{\sigma_\Delta}$ takes a nonzero value. For $p = 0$, α_c is known to be about 0.44. We obtained the threshold $\alpha_c(p)$ in Fig. 8 by seeing if the system enters the coherent state in a very long time (5×10^5 time units). For each value of α, $\overline{\sigma_\Delta}$ was calculated for ten independent samples. If the system reaches the coherent state ($\overline{\sigma_\Delta} = 0$) in every sample, we judge that $\alpha < \alpha_c$. If any one of the samples shows a nonvanishing value of $\overline{\sigma_\Delta}$ at $t = 5 \times 10^5$, then $\alpha > \alpha_c$. Figure 8 shows that the p dependence of α_c is nonmonotonic. For $0 < p < 0.0002$, increasing p lowers the threshold. For $p > 0.0002$, α_c slowly increases with p. For any $p > 0$, traveling waves are obtained just above α_c and are replaced by the chimera state at a larger value of α. Direct transition from the coherent to chimera states is found only for $p = 0$.

D. The effect of mobility for repulsive coupling

We next consider the effect of mobility for a repulsive coupling ($\alpha > 0.5$). In the absence of mobility, the spatiotemporal pattern consists of multiple domains of q-twisted states with positive and negative values of q, separated by incoherent strips. The range of the winding number is determined by a linear stability analysis [14], according to which the stable range of the phase difference is $0.215 < |\Delta| < 0.323$. (This corresponds to $54 < |q| < 80$ for a single-domain twisted state with $N = 500$.) Because of the large phase difference, it is much easier for the mobility to disturb the twisted states than in the attractive case. This explains the result that the system falls into complete incoherence except for small mobility ($p\,\delta t \ll 1$) as seen in Fig. 2. A typical spatiotemporal pattern in the small mobility region is shown in Fig. 1(h) where the disturbance effect is seen as noisy spots on the twisted domains. The threshold of the transition from the noisy pattern to complete incoherence can be again explained by the competition of the two timescales. The timescale of the decay of $\overline{\sigma_\Delta}(t)$ is on the order of ten time units and has only minor dependence on α as seen from Fig. 5(d). (Note that σ_Δ does not drop to zero in the steady state because of the coexistence of multiple domains. In this case, it would be reasonable to redefine $\tau_{\rm coh}$ by the time $\overline{\sigma_\Delta}$ decays to 0.5.) Meanwhile, the time for the system to become completely random in the absence of coupling follows Eq. (9). Here, we replace N/q with $2/\Delta$ and use the value of $0.215 < |\Delta| < 0.323$ to obtain

$\tau_{\text{rand}} \sim 10^{-2}/p$. Therefore, the two timescales are comparable to each other if p is less than the order of 10^{-3}, which is consistent with the threshold found in Fig. 2(b).

IV. DISCUSSION AND CONCLUSION

In this paper, we studied the combined effects of mobility due to random exchange of oscillators and frustrated coupling due to the phase lag. First, for $\alpha < 0.5$, we showed that the mobility enlarges the basins of attraction of twisted states with small $|q|$, including the fully synchronized state by destabilizing the twisted states with large $|q|$. This is reflected in the decay of the rms of q as a function of p. For $\alpha = 0$, we obtained the power law $\sigma_q \sim p^{-1/4}$, which is interpreted as follows. It is shown in a previous study of nonmobile oscillators [3] that the coupling range R and the standard deviation of q has the relationship $\sigma_q \approx 0.19\sqrt{N/R} - 0.11$, which reduces to $\sigma_q \sim R^{-1/2}$ for $R \ll N$. On the other hand, mobility effectively extends the coupling range. It is derived in Ref. [22] that $R_{\text{eff}} \sim p^{1/2}$ for large p, which means that the effective coupling range R_{eff} is given by the mean square displacement of each oscillator in a given microscopic time. Combining these two results, we obtain the power law $\sigma_q \sim p^{-1/4}$.

Second, we analyzed the timescales for randomization and restoring coherence by considering the mobility and coupling separately. The threshold mobility for destabilizing the q-twisted states is obtained by comparing the two timescales. For the attractive case, destabilization of a q-twisted states results in hopping to a basin of attraction of other q-twisted states with a smaller $|q|$, or the fully synchronized state. On the other hand, for the repulsive case, the coexistence of the q-twisted states with large $|q|$ is destroyed by small mobility, resulting in a fully incoherent state. Thus, mobility has opposite effects for the attractive and repulsive couplings.

Third, we found a meshlike pattern of traveling waves for the attractive coupling at the onset of incoherence. We suggest that local defects in the phase pattern caused by the exchange of oscillators trigger the traveling waves. For p close to 0, increasing p makes the traveling waves more easily generated, and, hence, the threshold α_c is lowered. For very large values of p, all the twisted states will be unstable, and only the synchronous state survives. In this case, the phase pattern is unaffected by the exchange of the oscillators, and no traveling waves can be generated. However, the precise mechanism of their formation is not clear and is left for future work.

In this paper, we considered a minimal model of mobile oscillators with a frustrated coupling. The mobility acts as a noise and induces hopping from metastable dynamical states to the globally synchronized state for the attractive coupling. For the repulsive case, the noise disturbs the chimera state and further enhances heterogeneity. We expect that these mechanisms are robust and valid in a wide class of coupled oscillators. including networks of immobile oscillators with dynamic rewiring. The results might find application in synchronization of mobile devices with delayed communication and neuronal network with rewiring. Neuronal networks show a plethora of heterogenous states that resemble the chimera states [9,10], whereas rewiring of synapses called structural plasticity contributes to homeostasis of brain activities [34]. A recent study showed that the structural plasticity strengthens both synchronization and desynchronization of neuronal firing [35], leaving simultaneous effects of rewiring and frustration an open question. We hope that the present paper will be extended to rewiring networks with frustration, including the neuronal system.

ACKNOWLEDGMENTS

This work was supported by JST, the establishment of university fellowships towards the creation of science technology innovation, Grant No. JPMJFS2102 to B.L., and by KAKENHI Grant No. JP21K03396 to N.U.

[1] M. Rosenblum and J. Kurths, *Synchronization: A Universal Concept in Nonlinear Science* (Cambridge University Press, Cambridge, UK, 2003).
[2] J. A. Acebrón, L. L. Bonilla, C. J. P. Vicente, F. Ritort, and R. Spigler, Rev. Mod. Phys. **77**, 137 (2005).
[3] D. A. Wiley, S. H. Strogatz, and M. Girvan, Chaos **16**, 015103 (2006).
[4] T. Girnyk, M. Hasler, and Y. Maistrenko, Chaos **22**, 013114 (2012).
[5] D. M. Abrams and S. H. Strogatz, Phys. Rev. Lett. **93**, 174102 (2004).
[6] Y. Kuramoto and D. Battogtokh, Nonlinear Phenom. Complex Syst. **5**, 380 (2002).
[7] M. J. Panaggio and D. M. Abrams, Nonlinearity **28**, R67 (2015).
[8] F. Parastesh, S. Jafari, H. Azarnoush, Z. Shahriari, Z. Wang, S. Boccaletti, and M. Perc, Phys. Rep. **898**, 1 (2021).
[9] S. Majhi, B. K. Bera, D. Ghosh, and M. Perc, Phys. Life Rev. **28**, 100 (2019).
[10] K. Bansal, J. O. Garcia, S. H. Tompson, T. Verstynen, J. M. Vettel, and S. F. Muldoon, Sci. Adv. **5**, eaau8535 (2019).
[11] Y. L. Maistrenko, A. Vasylenko, O. Sudakov, R. Levchenko, and V. L. Maistrenko, Int. J. Bifurcation Chaos **24**, 1440014 (2014).
[12] Y. Duguet and Y. L. Maistrenko, Chaos **29**, 121103 (2019).
[13] K. Kawase and N. Uchida, arXiv:1907.07285.
[14] B. Li and N. Uchida, Phys. Rev. E **104**, 054210 (2021).
[15] J. Buhl, D. J. Sumpter, I. D. Couzin, J. J. Hale, E. Despland, E. R. Miller, and S. J. Simpson, Science **312**, 1402 (2006).
[16] D. Tanaka, Phys. Rev. Lett. **99**, 134103 (2007).
[17] A. Buscarino, L. Fortuna, M. Frasca, and A. Rizzo, Chaos **16**, 015116 (2006).
[18] A. L. Christensen, R. O'Grady, and M. Dorigo, IEEE Trans. Evol. Comput. **13**, 754 (2009).
[19] F. Sivrikaya and B. Yener, IEEE Network **18**, 45 (2004).
[20] F. Peruani, E. M. Nicola, and L. G. Morelli, New J. Phys. **12**, 093029 (2010).
[21] N. Fujiwara, J. Kurths, and A. Díaz-Guilera, Phys. Rev. E **83**, 025101(R) (2011).

[22] K. Uriu, S. Ares, A. C. Oates, and L. G. Morelli, Phys. Rev. E **87**, 032911 (2013).
[23] J. Gómez-Gardeñes, V. Nicosia, R. Sinatra, and V. Latora, Phys. Rev. E **87**, 032814 (2013).
[24] A. Buscarino, L. Fortuna, M. Frasca, and S. Frisenna, Chaos **26**, 116302 (2016).
[25] N. Fujiwara, J. Kurths, and A. Díaz-Guilera, Chaos **26**, 094824 (2016).
[26] S. Majhi and D. Ghosh, Europhys. Lett. **118**, 40002 (2017).
[27] G. Petrungaro, K. Uriu, and L. G. Morelli, Phys. Rev. E **96**, 062210 (2017).
[28] K. P. O'Keeffe, H. Hong, and S. H. Strogatz, Nat. Commun. **8**, 1504 (2017).
[29] W.-H. Wang, Q.-L. Dai, H.-Y. Cheng, H.-H. Li, and J.-Z. Yang, Chimera dynamics in nonlocally coupled moving phase oscillators, Front. Phys. **14**, 43605 (2019).
[30] G. Petrungaro, K. Uriu, and L. G. Morelli, Phys. Rev. E **99**, 062207 (2019).
[31] L. A. Smirnov, M. I. Bolotov, G. V. Osipov, and A. Pikovsky, Phys. Rev. E **104**, 034205 (2021).
[32] R. Gopal, V. K. Chandrasekar, A. Venkatesan, and M. Lakshmanan, Phys. Rev. E **89**, 052914 (2014).
[33] R. Delabays, M. Tyloo, and P. Jacquod, Chaos **27**, 103109 (2017).
[34] M. Butz, F. Wörgötter, and A. van Ooyen, Brain Res. Rev. **60**, 287 (2009).
[35] K. Chauhan, A. Khaledi-Nasab, A. B. Neiman, and P. A. Tass, Sci. Rep. **12**, 15003 (2022).